The Vortex Formation of an Unsteady Translating Plate with a Rotating Tip

Juhi Chowdhury,* Luke Cook,† and Matthew J. Ringuette‡
University at Buffalo, The State University of New York, Buffalo, NY 14260 USA

We perform experiments to study the effect of a rotating tip surface on the outboard flow of a finite-aspect-ratio, high-angle-of-attack translating wing. Prior work on unsteady, translating wings showed that for rectangular planforms the tip vortex (TV) aids in the outboard leading-edge vortex (LEV) attachment, but the two are distinct. However, aft sweep promotes a connection between the outboard LEV and TV and potentially delays inboard LEV shedding. Moreover, rotating wings with low Rossby number exhibit LEV attachment, greater TV coherence, and higher lift. This paper examines whether a variable wingtip (panel) combining sweep and outward rotation, superimposed on the main-wing translation, can modify the adjacent, outboard LEV via an interaction with its swept-edge vortex (SEV), and affect the prior TV and trailing-edge vortex (TEV). The goal is a temporary lift boost, e.g. for a maneuvering unmanned aerial vehicle (UAV). The panel's ability to disrupt the outboard vortex formation during a streamwise gust-like motion (surge), via inward actuation to mitigate the lift increase, is also studied. Water towing-tank experiments are done with a wing of submerged aspect ratio 3.4, minus the panel, translating at 45° angle of attack and Reynolds number 10,000. Dye visualization via multiple injection ports, imaged using three orthogonal cameras, captures the 3D flow structure qualitatively. A starting flow and 50% streamwise gust after 21 chords are tested, with varying panel actuation timing, compared to a rectangular wing and static tip-sweep. In all cases, the main-wing speed divided by the forward tip speed, i.e. the advance ratio, is 0.95. For starting flows, outward tip-panel actuation at 0.1 chords traveled produces a new SEV, causes the TV and TEV to stretch outward and forward to follow the panel motion, and shifts the nearby-attached LEV outward; this should be beneficial for lift generation. For static tip sweep, the SEV appears to be less closely-attached. In both cases, the main LEV adjacent to the swept edge entrains SEV vorticity and temporarily weakens the SEV. Later tip actuation is less effective at modifying the flow structures, since this LEV interaction is exacerbated due to the larger LEV present when actuation starts. For the gust cases, inward panel actuation sheds the SEV and local TEV, and enhances LEV shedding similar to the rectangular wing. Also, it causes the aft TV flow to move inboard which is detrimental for lift. Actuation earlier, before the gust, has the greatest effect as it allows these phenomena to develop.

I. Introduction

The objective of the proposed paper is to investigate the ability of a variable wingtip geometry, specifically a rotating panel emerging from the main wing having aft sweep, to manage the outboard vortex-flow for wings in unsteady translation at high angles of attack (α). Ultimately, the application is to provide flow control for unmanned aerial vehicles (UAVs) during maneuvers and gusts.

Research on unsteady tip effects has focused on high-α wings in translation or rotation. At sufficiently-large α, wings in translation experience dynamic stall and the flow separates and rolls up into a leading-edge vortex (LEV) that generates high lift but then sheds,[1, 2] and strong tip vortices (TVs) also form along with a starting or trailing-edge vortex (TEV) [3]. Ringuette *et al.*[4] found that the TV increases the force on surging, low-$\mathcal{AR}$ normal flat plates in translation, and its low-pressure region aids in keeping the leading-edge vortices (LEVs) attached. Simulations by Jardin *et al.*[5] of 2-degree-of-freedom flapping wings in translation showed that the TV maintains LEV attachment, producing a local C_L increase. Shyy *et al.*[6] similarly showed that the TV downwash can "anchor" the LEV, creating locally low pressure and increasing lift, depending on the wing kinematics.

*Ph.D. Student, Department of Mechanical & Aerospace Engineering, 211 Bell Hall, Buffalo NY 14260, AIAA Student Member.
†Undergraduate Student, Department of Mechanical & Aerospace Engineering, 211 Bell Hall, Buffalo NY 14260.
‡Associate Professor, Department of Mechanical & Aerospace Engineering, 211 Bell Hall, Buffalo NY 14260, AIAA Member.

Taira and Colonius[3] simulated $\mathcal{AR} = 1-4$ wings translating from rest at post-stall α. They found that TV downwash adversely affects C_L, reducing it for lower $\mathcal{AR}$ as the TVs become more dominant; however, for $\mathcal{AR} = 1$ the TVs do keep the LEV perpetually attached [3]. For larger $\mathcal{AR}$, the LEV remains attached near the wingtips, but inboard it lifts off and exhibits an arch-like structure. Also, they showed that swept/curved wings connect the LEV and TV, promoting LEV-to-TV vorticity transport, delaying LEV shedding, and slightly delaying peak C_L [3]. Hartloper *et al.*[7] examined a translating and pitching plate via 3D particle tracking, finding that although the LEV and TV are distinct, the TV influence causes inboard LEV vorticity transport, reducing near-tip LEV growth.

For unsteady rotating wings, Lentink and Dickinson[8] found that low local Rossby number (*Ro*) promotes LEV attachment and higher C_L; they simplified *Ro* to aspect ratio ($\mathcal{AR}$) for small wing-root offsets. For *Ro* of $O(1)$, Coriolis accelerations are comparable to the inertial forces.[9] Wolfinger and Rockwell[10] examined *Ro* effects for an $\mathcal{AR} = 1$ rotating rectangular wing by increasing its radius of gyration, r_g, and thus increasing $Ro = r_g/c$ (c is chord length); $r_g\phi/c$ is the azimuthal distance traveled, with ϕ being the rotational angular position. For $Ro \approx 1$, the RV-LEV-TV loop is coherent even for $r_g\phi/c \approx 78$; RV is the root vortex. However, for $Ro = 5.5$, the loop moves away from the leading edge, and its coherence, including that of the TV which enhances LEV stability, degrades with larger $r_g\phi/c$ (approaching the translation case). Schlueter *et al.*[11] also found that with larger r_g the rotating-wing C_L is closer to the pure-translation case. Simulations by Jardin and David[12] showed that Coriolis effects are primarily responsible for close LEV attachment and high C_L, compared to centrifugal effects. Kruyt *et al.*[9] found that LEV attachment depends on $\mathcal{AR}$, occurring for $\mathcal{AR} < 4$, consistent with, e.g., Refs. [13–17]. A further discussion on *Ro* and LEV attachment with additional recent references is given in Sect. 2.

Regarding rotating-wing TV effects, for $\mathcal{AR} = 2.3$ Kim and Gharib[18] found that streamwise TV vorticity contributes to spanwise flow. For $\mathcal{AR} = 4$, Jardin *et al.*[5] showed that the LEV and TV connect, and LEV circulation saturates yielding constant local C_L. Wolfinger and Rockwell[10] commented that LEV stability is related to the interior RV and TV structure and the downwash they produce. Carr *et al.*[13] studied rotating $\mathcal{AR} = 2$ and 4 wings with small root offsets using stereo particle image velocimetry volume reconstructions, and showed that the $\mathcal{AR} = 2$ wing exhibits a more coherent and connected outboard LEV-TV flow despite the presence of breakdown, while both cases produce attached LEVs inboard. The C_L for each $\mathcal{AR}$ is similar, but impulse and lift calculations from the 3D data showed that for $\mathcal{AR} = 2$ the contribution from streamwise vorticity, due to the more coherent TV and outboard, aft-tilted LEV (and the low-pressure region they should create), is relatively higher.

Wing sweep effects on LEV attachment were explored using experiments with wings in translation or rotation [19–21], overall showing that sweep (and the resulting spanwise velocity) is insufficient to promote LEV attachment, but yields a stronger LEV-TV connection. Further, Wong and Rival [22] studied a plate executing a flapping motion in a freestream, and demonstrated that sweep does enhance LEV stability and vorticity transport along the span. Jardin and David[23] examined LEV attachment for finite-span wings, one subjected to a unidirectional freestream but with a spanwise velocity gradient, another in rotation. They found that a spanwise gradient aids in LEV attachment, but that the fictitious forces during rotation keep the LEV even closer to the wing and yield substantially greater lift. van Oorschot *et al.*[24] measured C_L for bird wings with outboard, static aft sweep either revolving or in a freestream. For forward flight, they found that sweep increases both $C_{L,max}$ and the α at $C_{L,max}$, while extended wings (extended from the bent, swept case) yielded higher C_L than swept wings during revolving. However, $\mathcal{AR}$ was not kept constant (for extended wings it increased by an average factor of 1.5 compared to swept wings, over all cases), making sweep effects difficult to interpret.

To summarize, TVs promote local LEV attachment for both translating and rotating wings, related to TV downwash. Aft wing sweep can increase LEV stability and outboard vorticity transport, facilitate an LEV-TV connection and axial vorticity transport, which also favors local LEV attachment. For rotating wings, spanwise velocity gradients and Coriolis effects for low *Ro* (and low $\mathcal{AR}$, for small wing root offsets) yield LEV attachment, TV coherence, and higher C_L. Throughout the Results section below (Sect. 3), further references are given in addition to those cited here, where applicable, for comparison with the present flow-visualizations features.

Example efforts on tip-flow control are briefly covered here. For steady freestreams, tip-flow control strategies include passive bleed [25], an aft tip flap with upstream fluidic perturbations [26], tip plasma actuators [27] and tip blowing [28], with success e.g. in modifying vortex topology [26, 28] and suppressing roll oscillations [25]. For $\mathcal{AR} = 2$ unsteady pitching, tip plasma actuators can increase lift by 40% [29]. For low-$\mathcal{AR}$ wings translating from rest, Taira and Colonius[30] found that steady trailing-edge blowing strengthens the TVs, which enhances downward flow over the LEVs, keeping them close to the wing and increasing C_L.

Also, Nicolic[31] studied the use of tip strakes, or half delta-wing (HDW) swept-tip shapes, for wings in steady freestreams with $\alpha < 25°$, similar to the shape proposed here but static. Depending on the strake and main-wing

incidence angles, a maximum lift-to-drag ratio or $(L/D)_{\max}$ increase of ~24% is achieved, presumably due to strake vortex lift. Lee and Pereira[32] examined the flow and forces of a HDW tip oriented at different angles. The HDW increases C_L and overall C_D, and can decrease induced drag and TV coherence; overall C_L/C_D is increased for high main-wing α. Although not directly applicable here, these studies show that enhanced lift and TV modification are possible.

The variable-tip geometry studied here is intended to potentially take advantage of two beneficial mechanisms described above: 1) aft tip-region sweep, which for finite-$\mathcal{AR}$ translating wings should promote a more coherent LEV-TV connection and vortex attachment; 2) local tip rotation (here done in the plane of the wing), which for rotating wings with low J and Ro produces LEV attachment, greater TV coherence, and higher lift. The hypothesis here is that a variable tip geometry that combines aft sweep and local tip rotation should yield a more connected and attached outboard LEV-TV for a high-α translating wing, thus temporarily boosting lift e.g. for a maneuver. This is accomplished via a movable tip panel (surface) that rotates outward from inside the main, rectangular translating wing. The panel has $\mathcal{AR} \approx 1$ and will have a low Ro. For the swept-edge tip geometry used here the distinction between the LEV and local TV can be ambiguous, therefore the term swept-edge vortex (SEV) is adopted, and for the trailing vortex immediately aft of it, TV will be used. A second set of tests is also done with the actuated tip panel rotating from an extended, swept-edge state to being retracted so that the tip geometry is rectangular. The objective of these experiments is the opposite: to determine the moving panel's ability to promote shedding of the SEV and outboard LEV, to reduce the increased lift (perturbation) from a streamwise, i.e. head-on, gust-like motion.

The goal of this paper is to begin to understand these flow interactions produced by the moving tip panel. The approach is to perform scaled experiments in a water tank for several cases. The 3D flow structure is captured qualitatively using multi-camera dye flow visualization. The main wing has a rectangular planform and its motion is an unsteady translation from rest for the starting-flow cases and a half-sine surge forward with an amplitude of 50% of the main-wing velocity after 21 chords traveled for the gust tests. For the starting-flow cases, the effects of outward panel rotation with aft sweep are examined, with two different panel-motion start times, to identify situations that may be beneficial for lift enhancement. For the gust study, inward panel rotation at two different times prior to the gust-like surge are investigated, to understand which has the greatest influence on the gust-induced flow structures and may be best for lift mitigation. Two reference cases with fixed planform shapes are examined for both sets of tests, representing the limits of the wing panel geometry: the main wing with no tip panel deployed (rectangular wing), and a static tip panel extended outward with constant sweep.

II. Experimental Setup and Methods

A. Facility, Wing Model, and Linear Motion

The experiments are conducted in a 4 m × 1.5 m × 1.1 m water towing-tank facility (Fig. 1a). It features uninterrupted glass walls, apart from a single cross-bar support at the bottom, is open at the top for model access, and is raised ~1 m above the ground on a steel frame with leveling feet, for optical access from below. The wing's linear motion is accomplished via a 3 m long linear brushless DC motor (H2W Technologies model DRS-120-08-006-01-EX). A programmable multi-axis Galil DMC4040 motion controller, using encoder feedback for each axis, controls the linear motor and tip-panel actuation motor. Galil Design Kit software is used to define and execute the simultaneous motion profiles.

The wing is mounted vertically in the tank from above, attached to the moving carriage of the linear motor (Fig. 1a). The wing pierces the free surface and, given that the free-surface deformations are small, this creates a nominally-2D end condition [33, 34]. The free surface can be treated as a reflected (symmetry) boundary [34], doubling the wing $\mathcal{AR}$. The rectangular main wing is made from two carbon-fiber composite plates epoxied together, with a chord length of $c = 8.1$ cm and submerged span of $b = 27.3$ cm. One plate is thicker and was machined with a cavity to accommodate the retracted tip panel, the moving rod that actuates it, and 3 internal brass dye tubes. A thinner cover plate was epoxied over this, giving a total thickness of 5 mm. The main-wing angle of attack is $\alpha = 45°$, to ensure a separated flow with a large LEV, and given the large body of literature on this condition. With the tip panel fully retracted, it has a submerged $\mathcal{AR} = b/c = 3.4$, doubled to 6.8 by the reflected free-surface boundary condition. A half-span $\mathcal{AR}$ greater than 2 is chosen so that a sufficient region of the inboard flow will not be substantially affected by the TV and will exhibit LEV shedding [3, 5]. In other words, so that the effects of the moving panel are not overwhelmed by having a low $\mathcal{AR}$ dominated by tip flow. The wing is ~8.9 chord lengths from each tank sidewall, and the tip when fully extended is ~7 chords from the bottom wall.

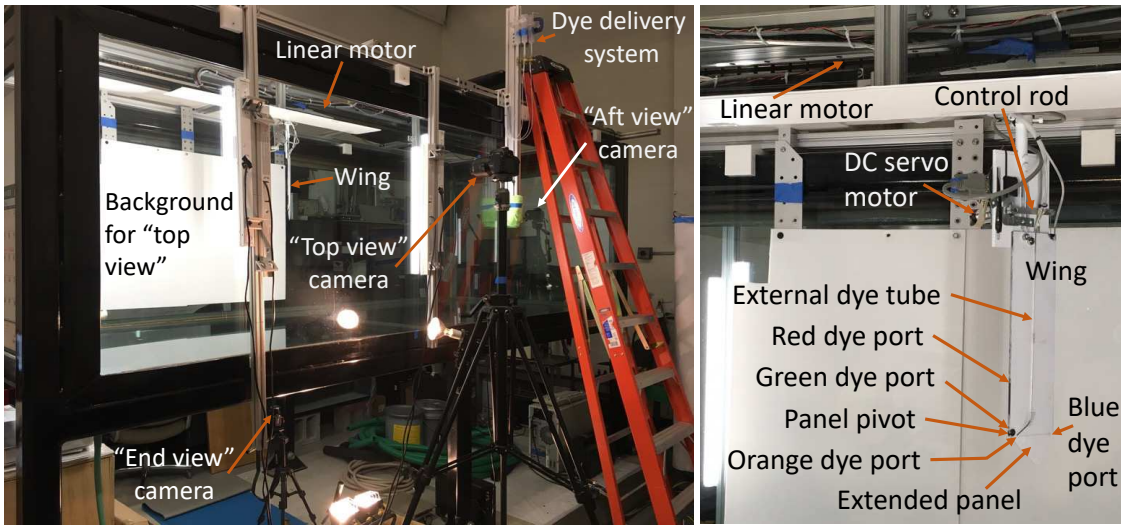

(a) (b)

Fig. 1 The experimental setup. (a) Towing tank facility, showing the linear motor, 3 cameras, lighting, backgrounds, dye gravity-feed system, and wing model. (b) Close-up of vertically-mounted wing model, with the DC servo-motor-controlled tip panel (extended), and multiple dye-injection ports.

The approximately 1/4-circle tip panel is made from a 1.63 mm thick carbon-fiber composite plate. It is attached inside the main wing to a pivot point near the main-wing leading- and tip-edge corner. The pivot location on the panel itself is near the apex of its 1/4-circle shape; its radius from the pivot point to its tip is $c_{\text{panel}} = 7.2$ cm. This pivot allows the tip panel to rotate outward from its completely hidden, retracted default position, where its leading edge is flush with the main-wing tip edge, or inward from an extended condition; Fig. 1b shows the fully-extended panel. The panel motion is actuated using a thin, stainless-steel push/pull control rod that travels primarily vertically but also laterally inside the main-wing cavity. One end of the control rod is connected to the aft corner of the tip panel for maximum actuation leverage, and the other is connected to a metal (radial) arm attached to the shaft of a brushed DC servo motor (Micromo model 2642W012CXRIE3-1024L+26A 16:1+MG26); the motor encoder has a resolution of 4,096 counts per revolution in quadrature. The motor and arm assembly are positioned above the free surface on the wing mounting assembly (Fig. 1b). The rod's radial attachment distance on the arm, 68.6 mm, is approximately equal to that where it attaches to the tip panel below, for simplicity of motion. The encoder and power cables of this motor, along with the silicone-rubber dye tubes supplying the wing dye manifold, are attached to the linear-motor cable bundle, all sliding along a support beam so that they move smoothly with the linear-motor carriage.

The motion profile for the main-wing translation for all starting-flow cases is a hyperbolic-tangent acceleration over $1c$ to a constant velocity of $U_{\text{main}} = 12.76$ cm/s, giving a Reynolds number of $Re = U_{\text{main}}c/\nu \approx 10,000$, where ν is the kinematic viscosity. The hyperbolic tangent acts to smooth the beginning and end portions of the acceleration phase. The wing travels a total distance of $8c$, then decelerates to a stop. The Re is chosen to be of the order appropriate for a small UAV [35]. For all gust cases, the same startup acceleration motion is used, reaching the same constant Re, however after $21c$ of travel the wing executes a half-sine velocity profile over a distance of $1c$ with a peak of $1.5U_{\text{main}}$; this is meant to emulate a strong, streamwise (head-wind) gust. Such streamwise gusts can be emulated by moving the model with respect to a constant freestream (including zero freestream) and are equivalent to a stationary wing with a streamwise perturbation in a wind tunnel, as long as care is taken to account for buoyancy effects for accelerating freestream cases [36–38]. A distance of $>20c$ is used to ensure more periodic LEV and TEV shedding prior to the gust, i.e. to mitigate startup effects, based on our preliminary force measurements (not shown) and due to tank length limitations; however, $>30c$ may be better [39, 40], although this likely depends on $\mathcal{AR}$ and Re. After the gust-like motion, which occurs over $1c$ of linear travel, the wing traverses another $7c$ before decelerating to a stop. The position accuracy of the linear-motor encoder is rated at 1 micron, however maximum deviations of about 100 microns, or $\sim 0.1\%c$, occur during the gust timing.

B. Tip Panel Motion

The angular position and velocity of the tip panel are $\theta(t)$ and $\dot{\theta}(t)$, respectively, relative the moving wing; $\theta(t)$ is measured from the rectangular wingtip edge. The exposed panel area, $S_{\text{exp}}(t) \approx \theta(t)c_{\text{panel}}^2/2$, is that extending from the main wing. The total submerged wing area is $S_{\text{wing,total}}(t) = bc + S_{\text{exp}}(t)$. When deployed, the panel increases the overall submerged wing $\mathcal{AR}$ to $(b + c_{\text{panel}} \sin\theta(t))^2/S_{\text{wing,total}}(t)$.

The tip panel experiences the superimposed main-wing translation, so a key parameter is the panel advance ratio J, defined following Refs. [8, 41] as $J = U_{\text{main}}/\left|(U_{\text{panel,tip}}\cos(\alpha))\right|$. The $\cos(\alpha)$ is needed since the panel's axis of rotation is oriented at α to U_{main}, the absolute value is required because the panel may rotate forward or backward, and note that $U_{\text{panel,tip}}$ does not include the superimposed U_{main}. Harbig *et al.*[42] examined the effects of J and $\mathcal{AR}$ for rotating wings in translation, and created a diagram of their J vs. $\mathcal{AR}$ cases showing which combinations produced a "stable" or "unstable" LEV (primarily attached or shed, respectively). Extrapolating their results to the low $\mathcal{AR} \approx 1$ tip panel of the present study, approximately $J < 2.25$ is required for the panel's LEV (here referred to as the SEV) to be attached.

Both Harbig *et al.*[42] and Lentink and Dickinson [8] discuss the problem in the context of *Ro* as well, stating that as long as the *Ro* remains low, which requires a small radial distance, attached LEVs are still possible in the presence of moderate-to-low wing forward motion or J. An attached and coherent LEV and TV have been found for rotating wings in a hover condition for about $Ro \leq 1.5$, with $Ro = r_g/c$, where r_g is the radius of gyration [8, 10]. Alternatively, in terms of local radial distance for rotating wings in hover with small root offsets (cutouts), an attached LEV has been found for approximately $r/c < 3$–4 [9, 43, 44]. In addition, there have been numerous rotating-wing studies showing the necessity of a low *Ro* for maintaining an attached LEV and high lift, and the further effects of $\mathcal{AR}$ and root offset (cutout) (a subset of very recent examples includes Refs. [43–46]).

The value used here is $U_{\text{panel,tip}} = 19$ cm/s, giving $U_{\text{panel,tip}} = 1.49U_{\text{main}}$ and $J = 0.95$. Therefore, according to Harbig *et al.*[42] the panel should be able to produce an attached LEV (SEV here). Also, with the small panel $\mathcal{AR}$ the *Ro* should be sufficiently low. The outward panel rotation starts at $\theta = 0°$ and reaches 45° after actuation, such that its aft LE sweep from the main-wing LE is 45°, while this is reversed for inward actuation. Due to the panel pivot being, by necessity, slightly away from the LE-tip corner of the rectangular main wing, the motor must rotate 46° to achieve the 45° panel rotation. The tip-panel velocity is a trapezoidal motion with acceleration and deceleration each occurring over 10% of the total motion duration, having a constant velocity of $U_{\text{panel,tip}}$ in between; the total duration of the tip motion is 0.3 s, and so it occurs over $0.47c$ of linear wing travel at U_{main}.

As indicated above, the goal of the outward tip actuation for the starting-flow cases is to temporarily boost lift by modifying the outboard main-wing LEV, TV, and TEV, in part through creating a new SEV. Of course the increase in wing area by $S_{\text{exp}}(t)$ and the associated fluid-inertial forces will add to the dimensional lift. In the future, force measurements to compare the lift coefficients of all cases, taking into account $S_{\text{exp}}(t)$, will aid in comparing the dynamic and static-geometry cases; here the study is limited to the flow-structures only. However, based on preliminary lift-force measurements (not shown here), for the starting-flow cases two actuation timings were chosen that were likely to substantially affect the vortex formation: actuation-out at $0.1c$ and $1.3c$ traveled by the main wing. The former occurs during the early LEV/TV/TEV formation, while the latter is at a time when a coherent LEV/TV/TEV have already formed. It is likely that the main effect of the outward panel deployment will be short-lived, however of interest is how long it takes for its overall influence to approach that of the fixed-sweep tip. For the gust cases, a streamwise surge will enhance the wing lift. Assuming this is an unwanted perturbation, actuation inward is examined in an attempt to promote LEV/SEV shedding and/or a loss of their coherence; the ultimate goal is to mitigate the lift increase. Again based on preliminary force measurements (not shown), two actuation timings were selected, prior to the gust start at $21c$: actuation-in at $18c$ and $20c$ traversed by the main wing. The force data indicate that earlier actuation inward may have the most effect.

For both the starting-flow and gust experiments, two reference cases with the same linear motion profiles and fixed tip geometries are tested for comparison: 1) the "rectangular" case for which the wingtip panel is fully retracted, and 2) the "swept" case where the wingtip panel is full extended to $\theta = 45°$. These represent the extremes of the actuated-tip planform geometries.

C. Dye Flow Visualization

Dye flow visualization with three simultaneous camera viewpoints is used to qualitatively capture and understand the 3D flow structure. The dye is a neutrally-buoyant mixture of food coloring, 2% milk, and 70% concentration ethyl alcohol, similar to that used by [47]. The colloids from the milk aid in inhibiting the mixture diffusion, and the alcohol is necessary to reduce the mixture density so it is neutrally buoyant, since the food-coloring density is greater than that

of water [48]. The dye is mixed with an equal amount of tank fluid, then prior to its use tests are done to determine if neutral buoyancy has been achieved. The wing has three embedded brass tubes. Two have exits flush with the leading edge at 70% and 95% span (with reference to the rectangular wing); these allow visualization of the LEV along the span. To mark vortices at the TE of the rectangular wing and over the aft region of the moving panel, a third brass tube exits outboard at the TE-tip corner. Further, a single stainless-steel tube of outer diameter 1.57 mm is attached to the wing suction side via 3 strips of packaging tape, which stays secured when submerged. It runs along the span near mid chord, then curves outward to exit flush with the rectangular tip edge, $0.14c$ aft of the panel pivot, to mark the SEV of the panel and the outboard LEV. Given its diameter and location primarily at mid-chord, it is expected to have a minimal influence on the wing flow; its external location is necessary, since internally it would interfere with the panel motion. Figure 1a shows the dye port locations. The dye is therefore delivered to regions of vorticity generation along the plate surface and to where it will be entrained by the vortices produced, to most effectively visualize the flow structures.

Different colors are used to distinguish the various flow features. The 70% and 95% leading-edge dye ports employ red and green dye, respectively, the TE-tip corner port uses blue dye, and the outer port near the panel pivot injects orange dye (Fig. 1b). An adjustable gravity-feed system delivers the dye to the metal tubes from reservoirs (Fig. 1a). Valves allow the reservoirs to be closed, and from the valves silicone tubing is run along the linear motor cabling and attached to the metal tubing of the wing at locations above the free surface. The flow rate is adjusted to be large enough to sufficiently mark the flow structures during the wing motion, but not so high that "jetting" and the associated instabilities are observed which would adversely affect the flow. For the starting flow, to mark the formation of the first vortex structures it is necessary to slowly inject dye blobs into the flow prior to the start of each run, as continuous injection is insufficient. Then, just prior to the run starting, the reservoirs are gradually lifted up to a height appropriate for continuous injection, so that the flow structures are visible throughout the run. Achieving these objectives requires iteration. For the gust motion, the reservoir height for sufficient, continuous dye injection is determined through testing. The gust motion is imaged starting at about $17c$ of linear wing travel. So that dye does not accumulate in the tank and block the aft-view camera, the dye is not deployed until a few chord lengths prior to this, upon which the reservoir is gradually raised to the proper height.

Lighting against white backgrounds is used to produce high-contrast images (Fig. 1a). The lighting consists of multiple, frosted white LED strip lights on the tank side walls, to illuminate side- and back-wall backgrounds and the wing itself; this is augmented from below by two halogen lamps. White backgrounds above the tank, including a small one on the wing carriage, are also used and take advantage of the halogens. A further spotlight illuminates the back-wall background to enhance the contrast for the aft-view camera, as it must image through the longest dimension of the tank. The wing suction side is also painted white to increase the dye visibility (Fig. 1b).

Given the 3D nature of the flow, multiple viewpoints are needed to properly understand its structure. During each run, three digital cameras with mutually orthogonal viewpoints simultaneously record the flow in high definition (Fig. 1a): one bellow the tank, viewing the vertically-oriented wing along the span from the tip (referred to as the "end view"); one imaging directly behind the wing from the back end of the tank ("aft view"); and one capturing the suction side of the wing from the side of the tank ("top view"). The end-view camera is a Canon Powershot SX510 HS with an f-number of 8, lens set at 100 mm, exposure time of 1/60 s, and recording images of 1920×1080 pixels^2 at 24 fps; the aft-view camera is a Nikon D3200 with an f-number of 11, lens set to 30 mm, exposure time of 1/1250 s, and recording images of 1280×720 pixels^2 at 60 fps; and the top-view camera is a Nikon D3400 with an f-number of 22, lens set at 70 mm, exposure time of 1/60 s, and recording images of 1920×1080 pixels^2 at 60 fps. The recordings are synchronized in post-processing using Sony Vegas Pro software, with reference to both an audio cue and the wing position. The time error is no more than ~6 frames for the Nikon cameras and ~2–3 for the Canon camera.

Post processing of the images includes basic image brightening and sharpening in cases where the lighting is slightly reduced, e.g. for the aft-view camera. This is done in a limited fashion to retain the maximum image information from the videos.

III. Results

A. Starting-Flow Cases

The starting-flow cases are presented first, and all figures show multiple images at the same time step. The four columns of images are for the different cases: fixed rectangular, fixed swept, and tip actuation-out at $0.1c$ and $1.3c$ traversed by the wing, respectively. The top, middle, and bottom rows give the three simultaneous camera views: top, aft, and end, respectively. The wing has the same scale in each row of images, but not across rows.

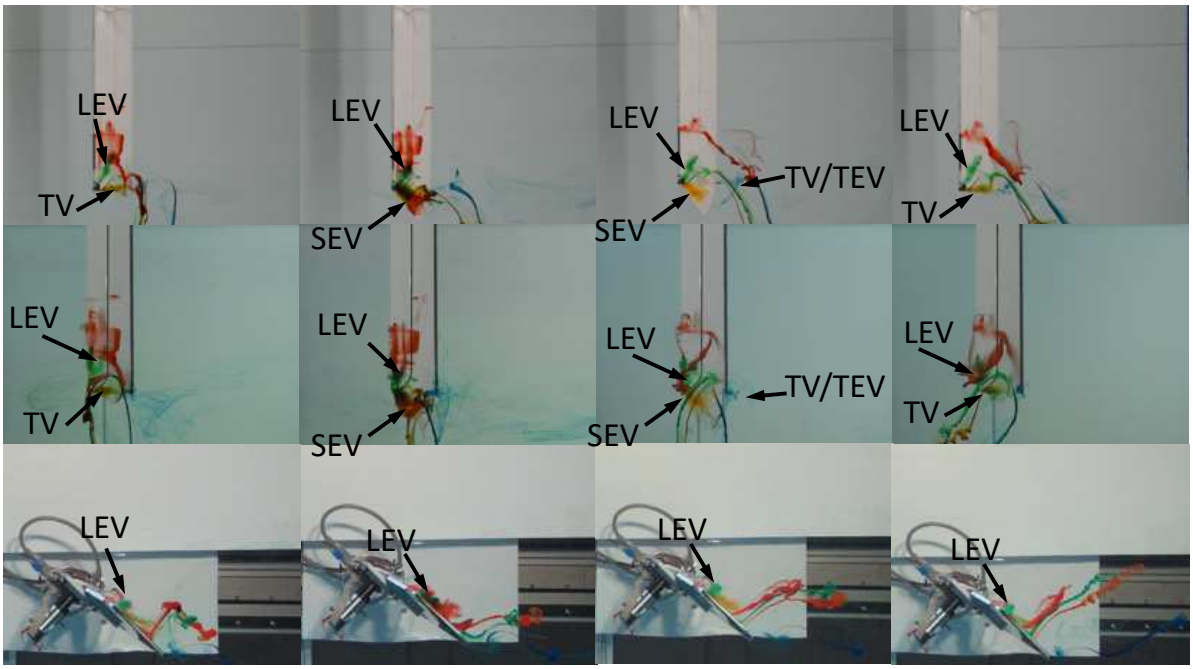

Fig. 2 The starting-flow structure at 0.77 translational chords traveled. The images show three simultaneous camera views of each case studied. The cases are given by column: (1) pure-rectangular; (2) static tip sweep; (3) tip rotation outward starting at $\sim 0.1c$ traveled; (4) tip rotation outward starting at $\sim 1.3c$ traveled. The rows give the camera views, namely, first row: top or suction-side view; second row: aft view, from behind the wing as it moves away; third row: end view, toward the wing tip.

Figure 2 gives the flow at $0.77c$ traveled by the wing. For the rectangular case, the first LEV formed is already aft of the LE inboard (red dye, top view), but outboard it is bent forward and pinned near the LE and tip-edge corner (green dye); this has been observed in several studies on finite-$\mathcal{AR}$ rectangular wings in either translation or freestreams, e.g. Refs. [3, 5, 19, 49–51]. Additionally, a second smaller LEV is visible ahead of the first, closer to the LE (red dye, top view); Jones *et al.*[49] and Jardin *et al.*[5] also found further LEV formation. Two similar LEVs are shown for the swept wing, as well. For the actuation cases, these two LEVs are present, however inboard less red dye was originally injected and therefore not entrained, so the first LEV is not as visible there, and the second LEV is only marked by a curled dye streak. In other repeated runs, not shown, the second LEV is more visible. In all cases, the LEVs exhibit substantial spanwise flow inboard, making them helical, as reported in prior work such as Refs. [4, 5, 7, 18, 50]. For the rectangular case, a TV forms along the tip edge (orange dye, top and aft views), and is deflected somewhat upward to be more parallel with the streamwise direction (orange dye, end view); the $1.3c$-actuation case is the same as that of the rectangular wing at this time, since the tip panel has not yet been deployed. The TV and LEV appear as separate structures, in that no observable dye is transported from one into the other. For rectangular planforms, the LEV and TV remaining distinct was also found by Taira and Colonius [3] and Hartloper *et al.*[7], and this feature is visible in the other work cited above. The swept-tip wing produces a large, attached and conical SEV, which has entrained previously-created blobs of red and green dye, in addition to the injected orange dye. It is similar to that of a delta wing, with axial flow directed outboard and aft [52]. Trailing this is a connected vortex referred to here as a TV. Just inboard of the SEV, the red and green dye show a connection between it and the adjacent LEV. This LEV-SEV-TV connection is consistent with the finite-$\mathcal{AR}$, aft-sweep results of Beem *et al.*[19].

For the $0.1c$ actuation-out case, the tip motion has recently completed by the time step shown in Fig. 2, and a conical SEV has formed over the tip panel (orange dye, all views). It is attached to the panel, and the dye indicates that perhaps it is more closely attached than the SEV of the fixed-sweep case (end view). This is difficult to ascertain, although a few time steps later the SEV of the fixed-sweep wing appears to grow somewhat larger and be less coherent. The aft TV flow (blue dye) marks primarily a TEV near the TE-tip corner at this early time for the rectangular and $1.3c$ cases (aft and end views). The blue dye for the swept tip also shows a TEV aft of the rectangular-portion TE, but more coherent and with inboard spanwise axial velocity (all views). This is due to the extended TE geometry of the swept case, with

respect to the blue dye port. Conversely, the TEV of the $0.1c$ actuation-out wing is stretched outboard in a curved shape, which somewhat mimics the outward rotational path of the tip panel.

Lastly, for the swept case and $0.1c$ actuation, the LEV near the tip is shifted outboard compared to the rectangular and not-yet-deployed $1.3c$ actuation wings; the green dye just above the curved injection tube shows this in each top view (Fig. 2). This is likely due to outboard flow from the developing SEV, and in the actuation case the induced flow from the panel. Given the comparable dye injection for the rectangular and actuated cases, although more dye is entrained for the swept tip, this is a real phenomenon and is also present in the repeated runs acquired. The LEV still appears to be attached near the LE-tip corner of the original rectangular geometry, which causes a local streamwise and aft LEV tilt. Another aspect of the swept and $0.1c$ actuation cases is that, compared to the rectangular wing, there is no TV near the LEV. Prior studies have shown that the rectangular-wing TV induces both a downwash and inboard flow that limit the LEV strength and promote its attachment [3, 5–7]. Removal of the local TV appears to allow the LEV to shift outboard, however the overall affect on the LEV strength is not clear due to the additional interaction with the SEV. A quantitative method such as particle image velocimetry (PIV) is needed to determine this, and moreover how the LEV and SEV strengths compare for the swept and actuated cases.

Overall, compared to the reference rectangular geometry, the tip actuation-out starting at $0.1c$ of travel may yield a more closely-attached SEV, stretches and shifts the connected TV-TEV outboard, and draws the near-tip LEV outboard (the latter two effects also progress into the next time step shown, Fig. 3). Closer SEV attachment will likely yield increased lift. Moreover, shifting the TV-TEV outboard (growing the trailing loop's projected area onto the horizontal) will increase the vorticity-moment in time, which will cause higher lift. Further, fluid-inertial effects from the changing geometry will affect the forces, as mentioned in Sect. 2. The LEV development and its potential influence on the lift is discussed more below. A thorough force measurement campaign is planned to assess these effects, and to analyze how the dynamic actuation case performs versus fixed sweep. It is likely that any benefits from actuation could be short-lived, however these may be sufficient for maneuvering purposes.

Next at $1.49c$ traversed, Fig. 3 shows aft travel of the first, largest LEV over the inboard portion of the wing for each case (red and green dye). Outboard, each LEV remains attached near the LE-tip corner region (top view), although for the fixed-sweep and $0.1c$ actuation-out wings, the LEV is shifted/tilted farther outboard as described earlier. Also for these cases, the movies show that their respective SEVs have begun to weaken. Inspection of the videos indicates that the core flow has started to become entrained into the nearby, growing LEV. For the swept case this is visible as green and orange dye from the SEV traveling inboard into the LEV, whereas for the $0.1c$ actuation wing the orange dye exhibits a similar behavior. As mentioned above, inboard axial LEV flow has been found in several studies on translating, rectangular wings. For aft-swept wings, there is typically a component of aft/outboard axial flow, see e.g. Ref. Wong2013. One reason for the behavior observed here may be that the LEV is simply dominant in terms of strength, creating a more intense low-pressure region compared to the SEV and driving the inboard axial flow. Another contributing factor could be that because the swept-edge of the tip panel is small at just under $1c$, the flow mechanisms associated with sweep may not have sufficient wing surface to develop with the presence of the growing LEV just inboard. This LEV is also progressing farther outboard in these cases at the time step shown (compare Figs. 3 and 4). Further, the swept geometry here is relegated to the tip, compared to the larger inboard rectangular wing, and also affected by the aft TV (see Fig. 4, top-view images). Lastly, the presence of a sharp corner in the planform geometry between the LE and swept edge may alter the connection and axial flow dynamics between the LEV and SEV, compared to a smoother curved shape.

Returning to the LE flow, for all cases in Fig. 3 the first and second LEVs continue to possess primarily inboard-directed axial velocity. Inboard of the tip where the first LEV is most tilted, there is some outboard spanwise velocity as the LE separated shear layer first rolls up into the tilted vortex. Whether the swept tip and/or actuated tip alter the LEV spanwise flow will require further investigation. At this time step, for $0.1c$ actuation the TEV (blue dye, top and aft views) continues its axial propagation and streamwise tilt to follow the tip panel, making it effectively a new TV. Also, for the $1.3c$ actuation case, the tip has started its motion and the SEV is just forming near the panel pivot location (orange dye).

At $1.88c$ traveled (Fig. 4), the tip-panel motion has recently completed for the $1.3c$ actuation, and an SEV (orange dye, all views) is visible, attached to the panel. Some of this dye is from the prior, rectangular-edge TV, which enlarged to follow the moving panel, whereas the aft portion of this TV did not move with the tip and is visible as an orange blob in the TE-tip corner. Unlike the $0.1c$ actuation at $0.77c$ of wing distance traveled (Fig. 2), for $1.3c$ actuation the TEV (blue dye) in the TE-tip corner does not stretch axially in an arc to follow the prior panel motion. Instead, the newly-injected blue dye from the port there is drawn outward along the panel TE; the previously-injected dye remains in the prior TV structure from the initially-rectangular geometry. This and the TV behavior (orange dye) indicate that

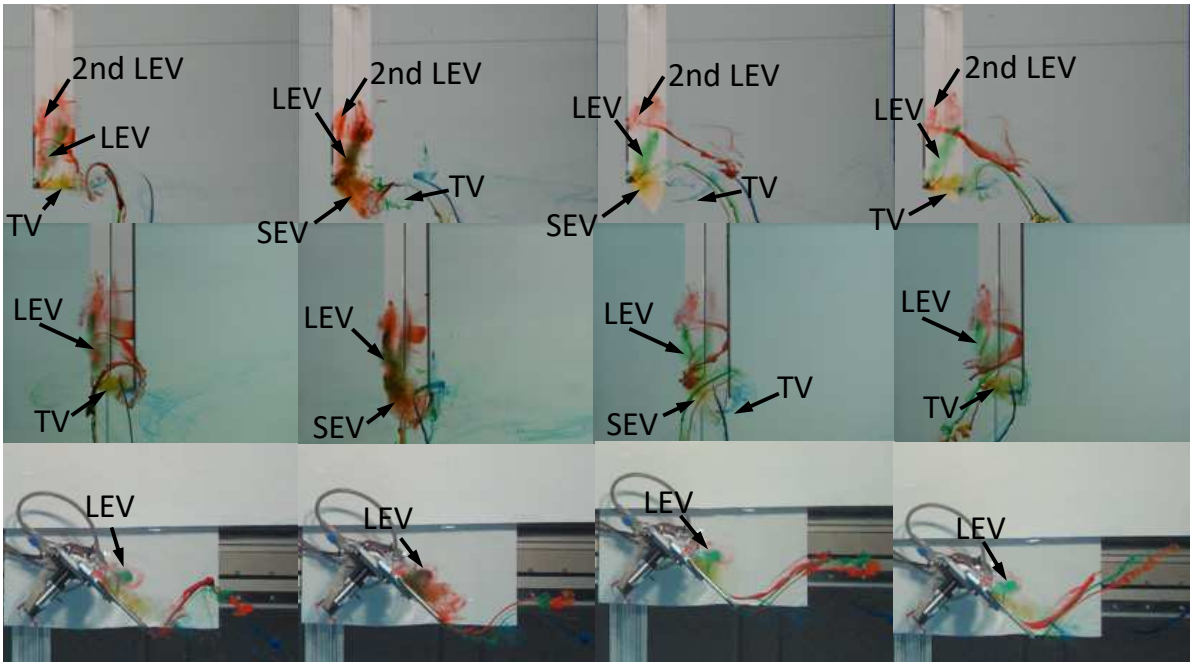

Fig. 3 The starting-flow structure at 1.49 **translational chords traveled. The key to the image organization is given in the Fig. 2 caption.**

the panel may be somewhat less effective in manipulating existing stronger vortices, versus the $0.1c$ actuation that occurs when the flow structures first form. As in the swept and $0.1c$ actuation cases, the LEV portion nearest the tip has begun to shift slightly outboard for the $1.3c$ action. Considering the $0.1c$ actuation again, the blue dye marking the newly-formed TV continues to follow the wing and be located aft of it, likely enhanced by axial stretching. The entrained dye blobs aft of the fixed, swept case show a similar aft TV flow. For the fixed sweep and $0.1c$ actuation, the entrainment of the SEV flow into the adjacent, inboard LEV, described earlier, has progressed: for the fixed-sweep wing it is the reduction of green dye in the SEV, for the actuated wing it is the lack of orange dye. In each case, the dye did not travel into the wake or appear to simply dissipate. With the absence of dye, it is unclear if a new SEV is concurrently forming for both configurations at this time from the forward flow over their swept tips; evidence of this is found later via the orange dye.

Regarding the LEV development, the inboard LEV for each case is lifted above the wing (green and red dye, top and aft views, Fig. 4). Outboard near the tip, the LEV for all configurations remains near the LE corner, although again it is farther outboard for the cases with swept tips. Moreover, for the fixed-sweep and $0.1c$-actuation cases, this outboard LEV is larger than for the rectangular and $1.3c$-actuation configurations. This size increase progresses with time for the swept and $0.1c$-actuation cases, at least through $3.4c$ traveled (Fig. 6), and is first visible later for the $1.3c$-actuation wing in Fig. 5 ($2.49c$ traveled), again compared to the rectangular wing. This greater growth of the attached, outboard LEV for the non-rectangular-tip cases should yield larger lift, although PIV and force measurements are required to compare the cases quantitatively. Just inboard of this, the LEV for all configurations is kinked further toward the wing as seen in the aft view (Fig. 4). The aft-view movies indicate that the likely cause is downwash from the large TV, visible via the motion of entrained dye blobs.

Later for $2.49c$ (Fig. 5), the inboard, first LEVs for each case have shed past the TE (top and end views), and due to the inboard spanwise velocity the dye has progressed farther toward the free surface. The LEVs for all cases have also grown in size and the kinked behavior described earlier has persisted. The outboard LEV shift near the tip is still present for the swept and actuated wings, compared to the rectangular geometry. The entrainment of the SEV core dye, which is green for the fixed-sweep case and orange for the $0.1c$-actuation, has progressed further; there is little visible dye over the tip panel for the $0.1c$ case. For the $1.3c$-actuation, this same phenomenon has occurred by this time, and the movies indicate its SEV from the panel deployment exists for a shorter time. This may be due to the tip motion occurring later, when the nearby LEV is already strong and its low pressure can cause relatively greater axial flow inboard. Considering the TV flow, it has grown longer aft for each case due to the wing motion, with several

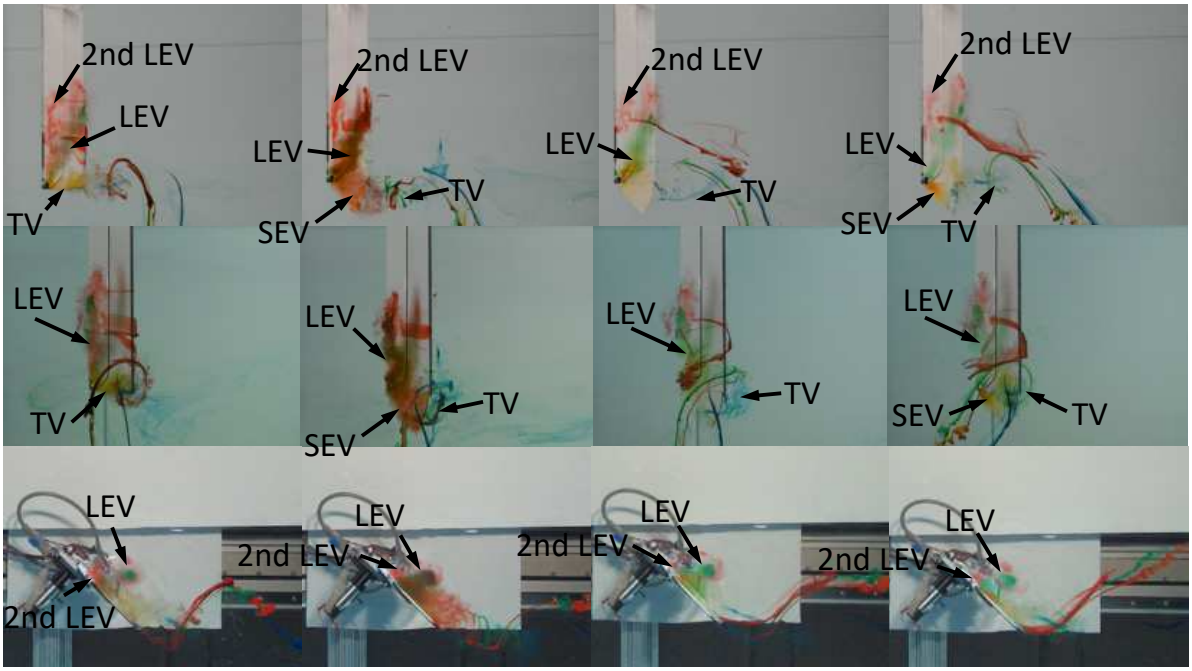

Fig. 4 The starting-flow structure at 1.88 **translational chords traveled. The key to the image organization is given in the Fig. 2 caption.**

smaller vortices are visible around it, from a Kelvin-Helmholtz-like shear layer instability that is typical for separated flows at this *Re* (e.g., see Ref. [13]). The aft portion of each TV is bowed more or less inboard, and likely connects to the main TEV of the wing, however no dye ports are available to show this. For the 1.3c-actuation case, the TV has shifted from being more aligned with the original rectangular tip edge to being aft of the newly-extended tip panel; as described above, this will contribute to increased wing lift.

As time progresses and the wing travels through 3.40c, 4.17c, and 6.40c (Figs. 6, 7, and 8, respectively) the inboard, main LEV for each case moves farther aft into the wing wake and lifts higher above the LE. Outboard, the LEV for all configurations remains closer to the wing. For the rectangular wing, the LEV is still pinned near the LE-tip-edge corner (top view). For the other cases with swept tips, the LEV is larger at the same spanwise position, i.e. near the tip location for the purely rectangular main wing (the larger LEV was discussed above). Overall, the main LEV becomes larger and more diffuse with time for each case, the visualization of which is confounded also by diffusion of the dye. At 4.17c, the red port marks only small LEVs forming (top and end views). Earlier at 3.40c traveled, the fixed-sweep and tip-actuated cases all exhibit similar flows, such that the effects from the tip motion are no longer observed. Additionally, blue dye from the TE-tip corner port has been entrained near the panel for each wing. At 4.17c of linear wing distance, orange dye is also visible from the port near the panel pivot point for these cases. These events mark the reestablishment of the SEV, which is finally visible for 6.40c traversed for the three wings with swept tips (orange and blue dye).

B. Streamwise-Gust Cases

The results of the streamwise-gust cases are given here, for which the wing surges forward at 21c traveled with a half-sine motion profile over a distance of 1c, and a peak velocity of 1.5U_{main}. The four cases are tip actuation inward at 18c and 20c traveled, and again the fixed rectangular and swept configurations for reference. Figure 9 shows the flow for each at 18.5c traversed. For all wings, numerous shed LEVs are visible via the red and green dye ports, respectively (top and end views). The rectangular wing exhibits a TV with multiple sub-structures, marked by orange, green, and blue dye, connected to a wake structure of dissipated dye that appears to be from a previously shed LEV system. As expected, the swept and 20c-actuation cases have a helical SEV (orange dye) with axial flow outboard along the edge, similar to a delta wing. The tip flow is less prominent than for the rectangular wing, due to the lack of a tip edge parallel to the wing motion (in the top-view sense), with numerous small vortices being shed (orange and blue dye). For the 18c-actuation, at this time the tip panel has nearly completed its retracting motion. The previously-created SEV (orange)

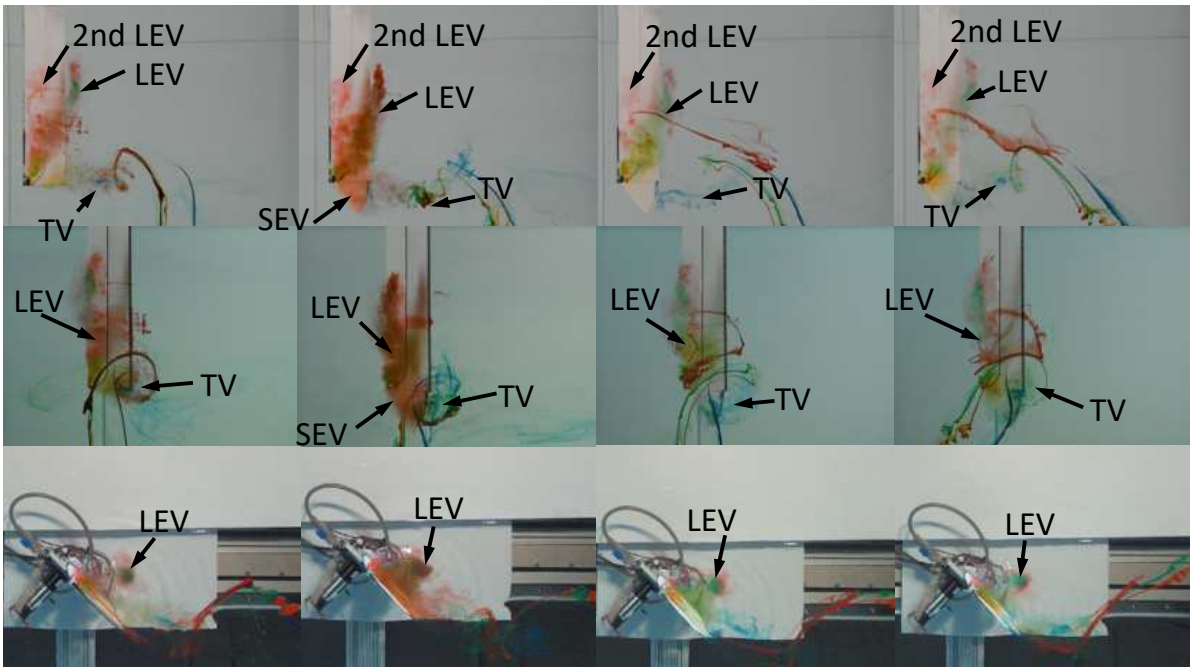

Fig. 5 The starting-flow structure at 2.49 **translational chords traveled. The key to the image organization is given in the Fig. 2 caption.**

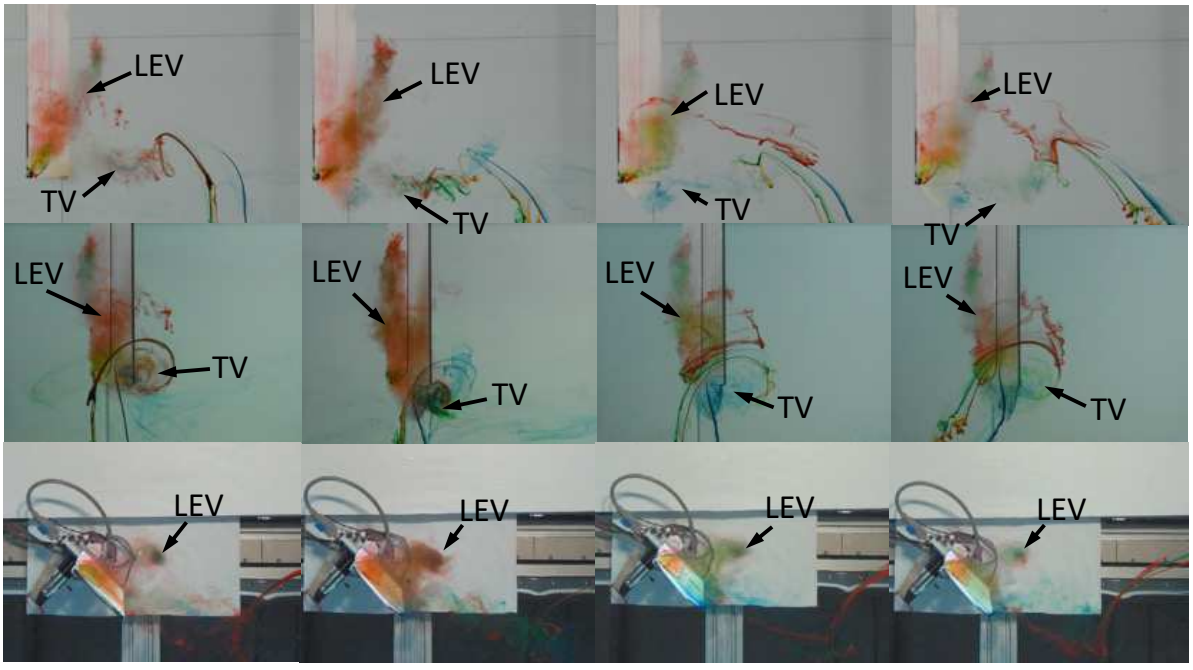

Fig. 6 The starting-flow structure at 3.40 **translational chords traveled. The key to the image organization is given in the Fig. 2 caption.**

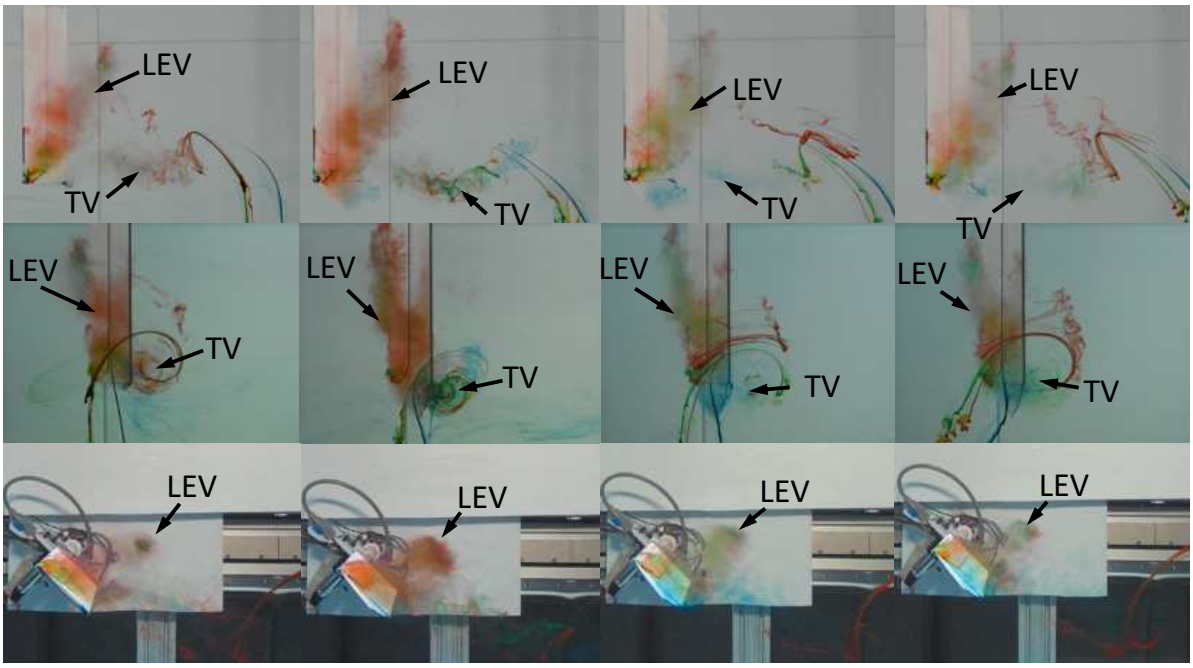

Fig. 7 The starting-flow structure at 4.17 **translational chords traveled. The key to the image organization is given in the Fig. 2 caption.**

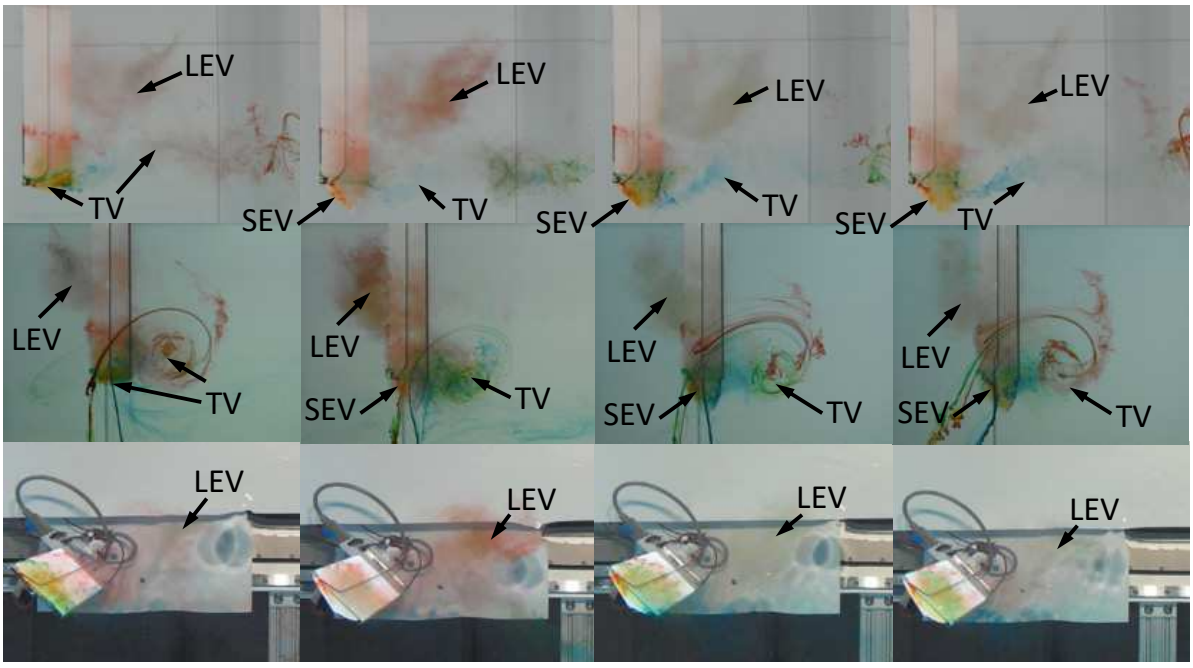

Fig. 8 The starting-flow structure at 6.40 **translational chords traveled. The key to the image organization is given in the Fig. 2 caption.**

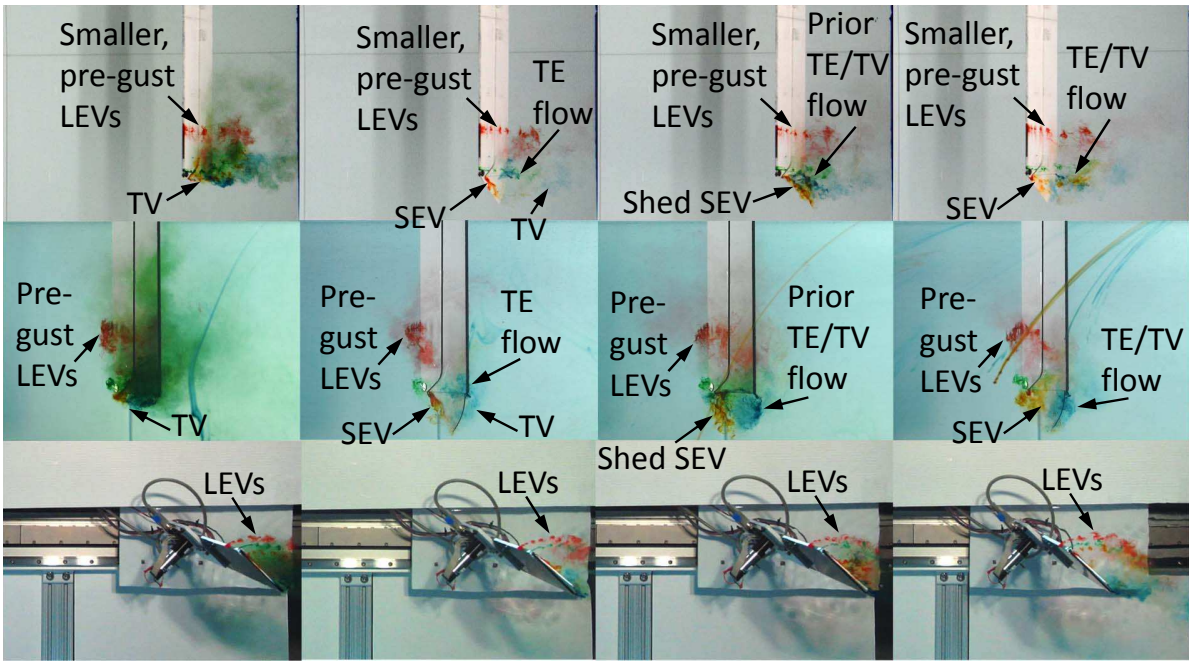

Fig. 9 The gust-flow structure at 18.5 **translational chords traveled. The key to the image organization is given in the Fig. 2 caption, except that columns (3) and (4) are for tip rotation inward starting at** 18c **and** 20c **traveled, respectively.**

is shed and remains close to its original position, but has begun to be drawn inboard by the flow created from the panel motion. The panel movement also causes some blue dye in the tip-TE flow to travel inboard, closer to the SEV. The two form a somewhat coherent loop (aft view), which geometrically resembles the outline of the originally-extended panel.

Continuing with the 18c-actuation-in case, the movie shows that the aft part of the tip-region loop (blue dye, Fig. 9) is brought closer to the shed SEV (orange) by the panel-induced inboard flow. Since they have opposite swirling directions, some vorticity annihilation must occur. Afterward, the two travel into the wake, with the blue-dyed vortex moving outboard and with visibly weaker swirl, while the stronger orange-marked structure proceeds inboard as it travels aft. This finally leads to the time step of Fig. 10, which shows each case at 20.5c traveled, still prior to the gust surge. The orange-marked shed vortex has shifted substantially inboard, essentially leaving a time-trace of the effect of the inward tip panel actuation, where it interacts with shed LEVs (red dye). This inboard motion of the aft TV flow, which is not observed in the fixed-geometry cases though it is found later for the 20c-actuation, reduces the size of the shed vortex loop as viewed from above the wing, which will act to decrease the vorticity moment and lift. Nearer to the tip, for the 18c-actuation case the flow relaxes to a state closer to the rectangular wing, which itself continues to shed small- and large-scale LEV and TV structures (top and end views). At this time step, the swept configuration is unchanged except for further shedding. For the 20c-actuation, the tip panel has completed its retraction. Similar to the earlier 18c-actuation case, a visible loop remains near the original tip-panel boundary, consisting of the previously-formed SEV (orange dye) and TE vorticity (blue dye, see the top and aft views, and compare with the swept case, Fig. 10).

Figure 11 shows each flow at 22.4c traversed, just after the gust motion has completed. For the rectangular case, the forward surge produces a new, strong and coherent LEV (marked by orange, green, and red dye), with substantial inboard spanwise flow and being pinned near the LE-tip-edge corner. Also created is further tip vorticity, visible near the wing via orange and green dye, and aft from the blue dye. A new, more intense TEV is generated as well, which connects to the aft TV (blue, top view). Overall, vortex structures resembling those of the starting flow are formed by the surge, although in the presence of the prior shed vorticity. This is in agreement with the time-resolved PIV and force measurements of Mulleners *et al.*[39] on an $\mathcal{AR} = 6$ translating wing comparing a surge from rest with that after 30c traveled, which showed that in both cases the flow features from the surge and the lift-force decay were similar. For the swept configuration, all views show that the gust similarly produces a strong LEV inboard (red dye) with inboard spanwise velocity, and a new, coherent TEV (blue dye). Moreover, a large, conical SEV is created early in the gust motion (orange dye, top view), although the end view shows that by this time it has shed from the wing, likely due to the

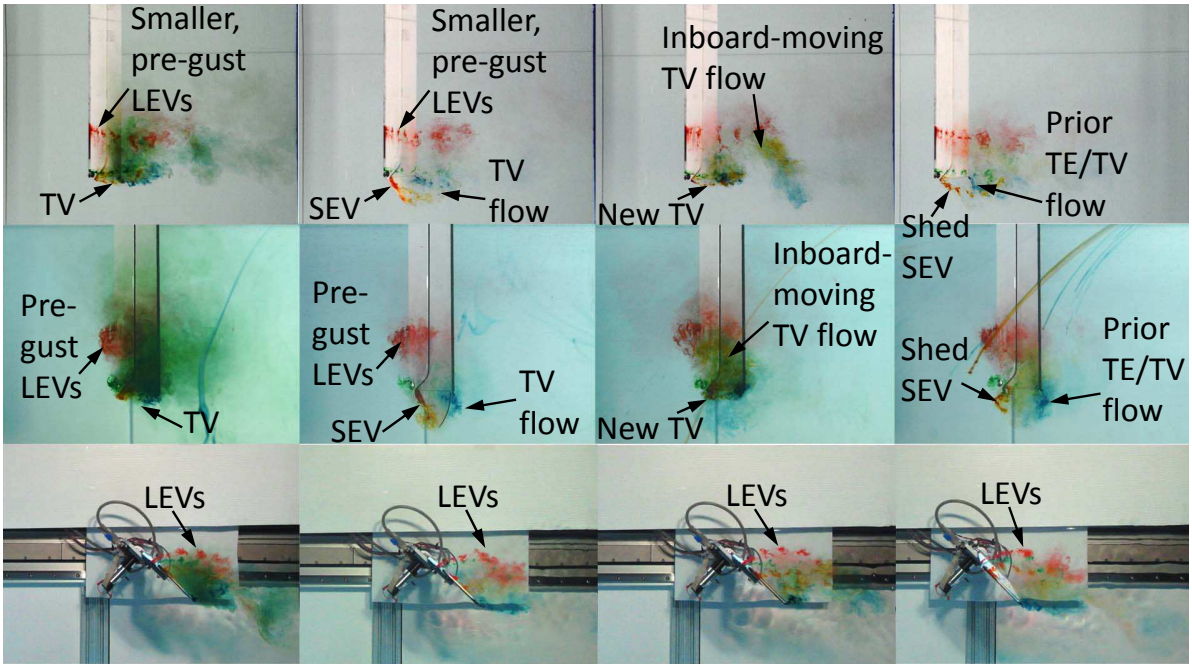

Fig. 10 The gust-flow structure at 20.5 **translational chords traveled. The key to the image organization is given in the Fig. 9 caption.**

deceleration at the end of the gust, and connected inboard to the LEV (orange, green, and red, dye, top and aft views). Again, these features are akin to those of the starting flow.

For the 18c actuation case, the aft TV flow proceeds farther inboard, which again is detrimental for lift, compared to the swept case which maintains the initial tip geometry of the actuated wing (Fig. 11); recall that the goal for the actuation here is to reduce the lift. Near the wing tip, the 18c-actuation flow is similar to that of the rectangular case. The 20c-actuation flow exhibits some of the inboard wake motion of the 18c-actuation wing, but its progression is limited due to the later tip-motion start. Locally to the wing, the 20c actuation flow also resembles that of the rectangular case. The end view shows that the gust-generated inboard LEV (red and green dye) is in a similar position above mid-chord for each case, indicating that the strong perturbation has the same effect inboard. It also indicates that the gust-produced TEV (blue) is farther below the wing, more coherent, and slightly more aft for the swept case, which will aid in lift generation. The TEV is somewhat closer to the wing for 20c-actuation, and nearest for the rectangular and 18c-actuation wings (Fig. 11).

Further after the gust motion, for 23.2c of wing travel, the flow of the actuation cases still does not fully resemble that of the fixed rectangular wing, despite them having finally assumed that geometry (Fig. 12). This indicates that the actuation effects persist through the surge. The differences are greater for the earlier 18c actuation versus 20c, because further time is allowed for the flow produced by the panel motion to progress. The former has a larger aft TV (blue dye, top view), generated during the gust, also compared to the fixed rectangular wing; whether this TV is stronger or weaker than those of the other cases requires further information from e.g. PIV. Additionally, the inboard motion of the aft TV flow of the 18c-actuaton case, formed prior to the gust, has advanced more than that of the 20c-actuation. The fixed rectangular geometry also exhibits inboard motion of the aft TV flow. This is likely caused by induced flow from the TV, which must also be a factor in the actuation cases. Considering again the 18c-actuation, the inboard travel of the aft TV formed before the gust makes it bow-shaped (blue and green dye, top and aft views). It is likely stretched and enhanced by the inboard flow from the panel actuation; this is less-pronounced for the 20c-actuation. For the swept case, two blue-dyed TEVs are visible, oriented similar to the panel TE (top and aft views); the one farthest aft is produced by the gust motion, the one closest to the wing forms afterward. Also, for this configuration a new SEV has started to be reestablished (orange, top and aft views).

The gust-generated LEV in each case continues to exhibit strong inboard flow and be helical (red and orange dye, top and aft views of Fig. 12). Considering the inboard LEV portion, for the 18c-actuation it has traveled as far aft as that of the rectangular wing, whereas for the swept and 20c-actuation flows it is closer (top view). The aft view further

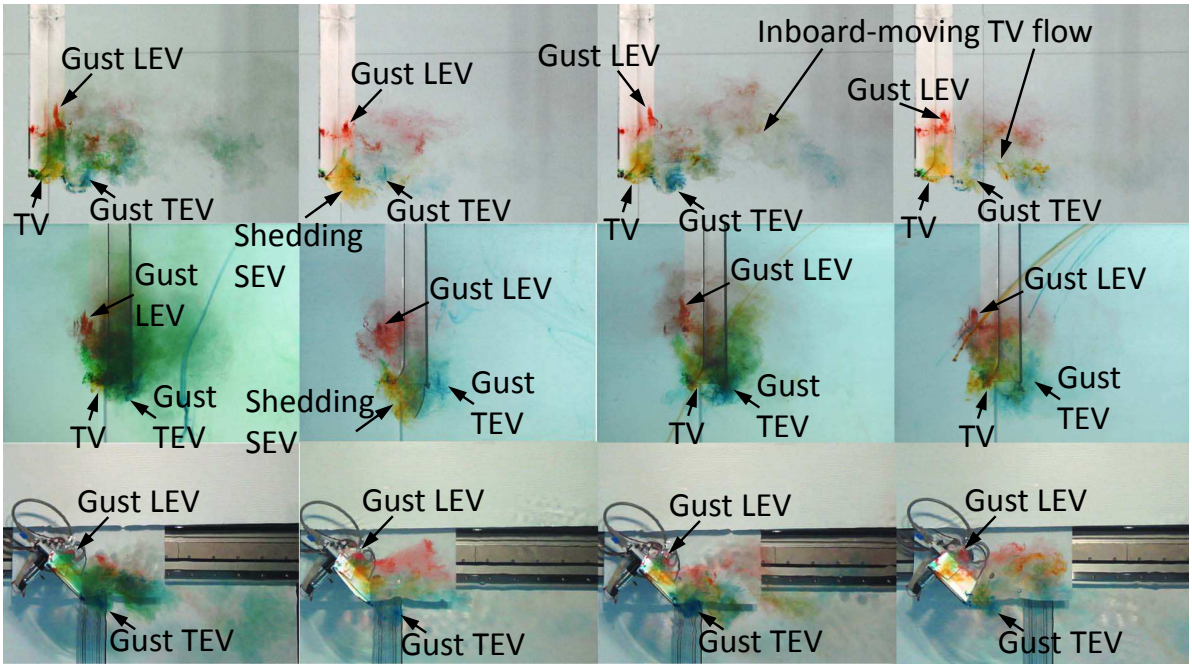

Fig. 11 The gust-flow structure at 22.4 translational chords traveled. The key to the image organization is given in the Fig. 9 caption.

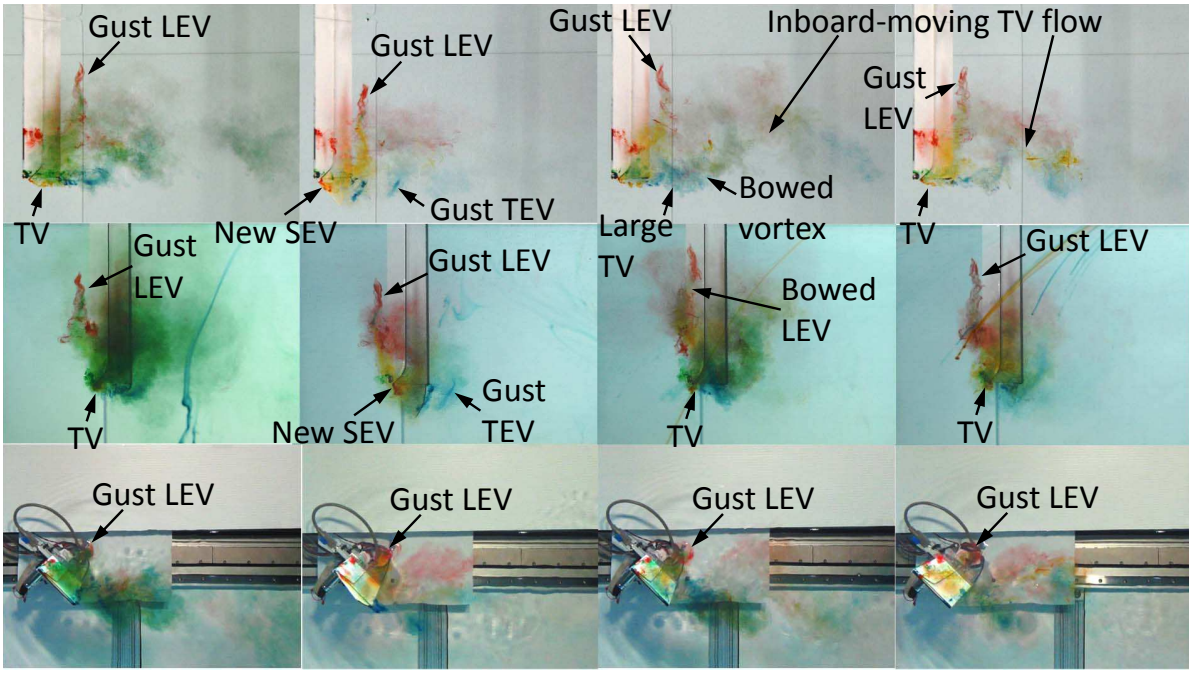

Fig. 12 The gust-flow structure at 23.2 translational chords traveled. The key to the image organization is given in the Fig. 9 caption.

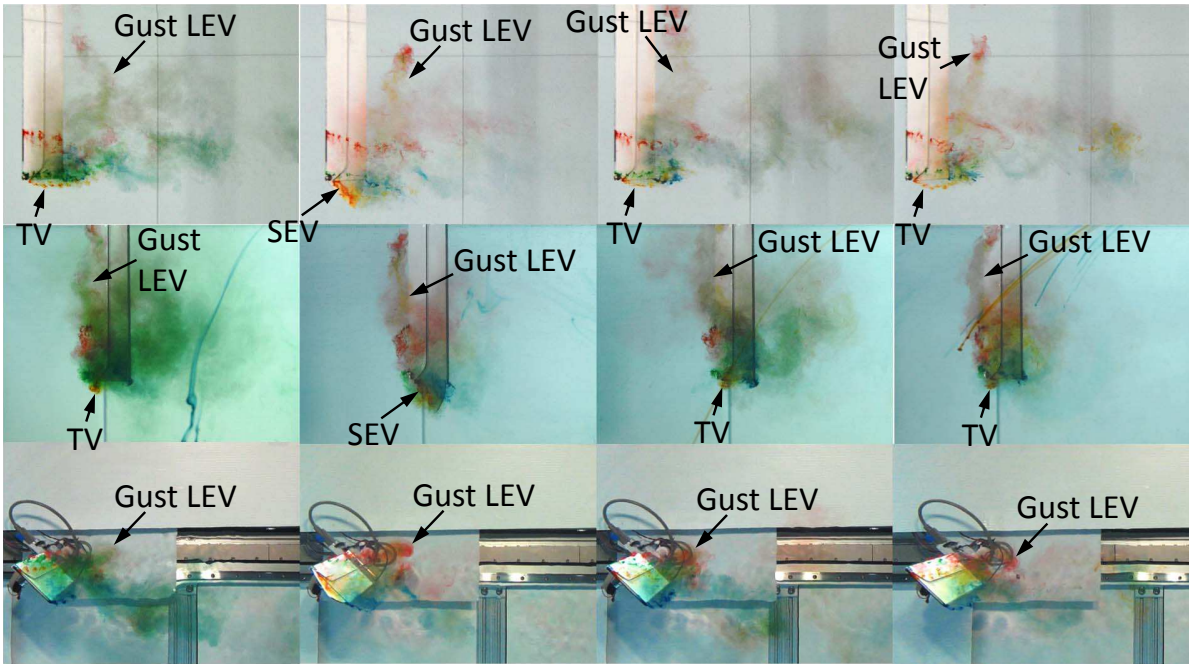

Fig. 13 The gust-flow structure at 24.8 **translational chords traveled. The key to the image organization is given in the Fig. 9 caption.**

shows that the inboard LEV for 18c-actuation is bowed into an arch. Overall, in terms of position above or below the LE, this LEV is nearest to the LE location over much of its length, and farther inboard it is below the LE (aft view). For the other cases, inboard of the tip region the LEV is lifted above the wing. Near the tip, the LEV for the rectangular, 18c-, and 20c-actuation cases is kept close to the wing despite shedding inboard (top and aft views), which bows the LEV toward the tip. This is likely from downwash due to the strong TV produced at the tip edge of the rectangular geometry, which in the top view is aligned with the wing motion. Conversely, although the swept case produces an SEV, it is lifted off at this time, and moreover the swept tip has a pointed geometry. These lead to a less-coherent tip flow, reducing the downwash effect, so that the LEV in the tip region is shifted farther aft and above the plate.

Later at 24.8c traveled (3.8c after the gust is initiated, Fig. 13), for the rectangular case the LEV that formed during the gust has shed and started to dissipate (green and red dye, top view). For the swept case, the SEV is reestablished (orange dye, all views), perhaps due to the shedding of the gust-surge LEV which might otherwise entrain some of its vorticity, and the shed LEV is more coherent inboard. The 20c-actuation flow exhibits a shed LEV similar to that of the swept case (red and orange dye, top and aft views), and shed TV-TEV behavior resembling the rectangular wing. The aft-view movies for the 18c-actuation and rectangular cases show strong TV flows and downwash, which bend the LEV toward the TE (in the aft-view sense) inboard of the tip, as mentioned earlier. This effect is much less pronounced for the swept tip with its weaker TV flow, as well as for the 20c-actuation case. It is not clear from the movies how the shed LEV interacts with the TV outboard. There are likely complex vortex connections and wrapping in this region, but with the diffuse dye at this time and at the *Re* chosen, these features are difficult to discern and further study is needed.

IV. Concluding Remarks

This paper investigates the ability of a rotating, low-$\mathcal{AR}$ and aft-swept tip panel, superimposed on a translating main wing, to manage the outboard LEV and TV flow for both a starting flow and a superimposed 50% streamwise gust occurring at 21 chords traveled. For the starting flow, the ultimate goal is a temporary boost in lift, whereas for the gust case the aim is to reduce the lift increase from the streamwise surge. Scaled experiments at Reynolds number of 10,000 in a water towing tank are used, and the 3D flow structure is captured qualitatively from dye flow visualization with three orthogonal camera views. For the starting-flow case, early panel actuation outward at 0.1 chords traveled produces an SEV, makes the connected TV and TEV stretch to trace the arc of the panel movement, and slightly displaces the tip-region attached LEV outboard while also causing it to grow larger, compared to the purely-rectangular

wing. These phenomena should be beneficial for producing lift. For the fixed-sweep case, an SEV is also generated, although it may not be as closely-attached versus the dynamic tip, and an outboard-shifted, larger LEV is also found. In both the fixed-sweep and actuation-out configurations, the LEV near the swept edge entrains the SEV's vorticity and temporarily, but significantly, weakens it. Actuation-out later is less effective at changing the flow structures, since this LEV interaction is stronger due to the larger LEV formed when the actuation starts. For the gust cases, inward panel motion sheds the SEV and promotes LEV shedding similar to the rectangular-wing configuration. Moreover, it causes the aft TV flow to travel inboard which will reduce lift. The actuation time must be early enough to modify the flow prior to the occurrence of the gust. In the future, force measurements will be correlated to the flow behavior to quantitatively compare the performance of each case.

Acknowledgments

We would like to thank Stephen Gagnon and Olivia Gustafson for their help with the initial wind design and testing, and Luke Cook for assistance in setting up and executing the dye flow visualization. This work is supported by the National Science Foundation, award no. CBET-1706453, supervised by Dr. Ronald Joslin.

References

[1] McCroskey, W. J., "Unsteady Airfoils," *Annual Review of Fluid Mechanics*, Vol. 14, No. 1, 1982, pp. 285–311. doi: 10.1146/annurev.fl.14.010182.001441, URL https://doi.org/10.1146/annurev.fl.14.010182.001441.

[2] Dickinson, M. H., and Gotz, K. G., "Unsteady Aerodynamic Performance of Model Wings at Low Reynolds Numbers," *Journal of Experimental Biology*, Vol. 174, No. 1, 1993, pp. 45–64. URL http://jeb.biologists.org/content/174/1/45.

[3] Taira, K., and Colonius, T., "Three-dimensional flows around low-aspect-ratio flat-plate wings at low Reynolds numbers," *Journal of Fluid Mechanics*, Vol. 623, 2009, p. 187–207. doi:10.1017/S0022112008005314.

[4] Ringuette, M. J., Milano, M., and Gharib, M., "Role of the tip vortex in the force generation of low-aspect-ratio normal flat plates," *Journal of Fluid Mechanics*, Vol. 581, 2007, p. 453–468. doi:10.1017/S0022112007005976.

[5] Jardin, T., Farcy, A., and David, L., "Three-dimensional effects in hovering flapping flight," *Journal of Fluid Mechanics*, Vol. 702, 2012, p. 102–125. doi:10.1017/jfm.2012.163.

[6] Shyy, W., Trizila, P., kwon Kang, C., and Aono, H., "Can Tip Vortices Enhance Lift of a Flapping Wing?" *AIAA Journal*, Vol. 47, No. 2, 2009, pp. 289–293. (Aerospace Letters).

[7] Hartloper, C., Kinzel, M., and Rival, D. E., "On the competition between leading-edge and tip-vortex growth for a pitching plate," *Experiments in Fluids*, Vol. 54, No. 1, 2013, p. 1447. doi:10.1007/s00348-012-1447-5, URL https://doi.org/10.1007/s00348-012-1447-5.

[8] Lentink, D., and Dickinson, M. H., "Rotational accelerations stabilize leading edge vortices on revolving fly wings," *J Expl Biol.*, Vol. 212, 2009, pp. 2705–2719.

[9] Kruyt, J. W., van Heijst, G. F., Altshuler, D. L., and Lentink, D., "Power Reduction and the Radial Limit of Stall Delay in Revolving Wings of Different Aspect Ratio," *J. R. Soc. Interface*, Vol. 12, 2015, p. 20150051.

[10] Wolfinger, M., and Rockwell, D., "Flow structure on a rotating wing: effect of radius of gyration," *Journal of Fluid Mechanics*, Vol. 755, 2014, p. 83–110. doi:10.1017/jfm.2014.383.

[11] Schlueter, K. L., Jones, A. R., Granlund, K., and Ol, M., "Effect of Root Cutout on Force Coefficients of Rotating Wings," *AIAA Journal*, Vol. 52, No. 6, 2014, pp. 1322–1325. doi:10.2514/1.j052821, URL https://doi.org/10.2514/1.J052821.

[12] Jardin, T., and David, L., "Coriolis effects enhance lift on revolving wings," *Phys. Rev. E*, Vol. 91, 2015, p. 031001. doi:10.1103/PhysRevE.91.031001, URL https://link.aps.org/doi/10.1103/PhysRevE.91.031001.

[13] Carr, Z. R., DeVoria, A. C., and Ringuette, M. J., "Aspect-ratio effects on rotating wings: circulation and forces," *Journal of Fluid Mechanics*, Vol. 767, 2015, p. 497–525. doi:10.1017/jfm.2015.44.

[14] Luo, G., and Sun, M., "The effects of corrugation and wing planform on the aerodynamic force production of sweeping model insect wings," *Acta Mechanica Sinica*, Vol. 21, No. 6, 2005, pp. 531–541. doi:10.1007/s10409-005-0072-4, URL https://doi.org/10.1007/s10409-005-0072-4.

[15] Harbig, R. R., Sheridan, J., and Thompson, M. C., "Reynolds number and aspect ratio effects on the leading-edge vortex for rotating insect wing planforms," *Journal of Fluid Mechanics*, Vol. 717, 2013, p. 166–192. doi:10.1017/jfm.2012.565.

[16] Garmann, D., and Visbal, M., "Dynamics of revolving wings for various aspect ratios," *Journal of Fluid Mechanics*, Vol. 748, 2014, p. 932–956. doi:10.1017/jfm.2014.212.

[17] Phillips, N., Knowles, K., and Bomphrey, R. J., "The effect of aspect ratio on the leading-edge vortex over an insect-like flapping wing," *Bioinspiration & Biomimetics*, Vol. 10, No. 5, 2015, p. 056020. URL http://stacks.iop.org/1748-3190/10/i=5/a=056020.

[18] Kim, D., and Gharib, M., "Experimental Study of Three-Dimensional Vortex Structures in Translating and Rotating Plates," *Exp. Fluids*, Vol. 49, 2010, pp. 329–339.

[19] Beem, H. R., Rival, D. E., and Triantafyllou, M. S., "On the stabilization of leading-edge vortices with spanwise flow," *Experiments in Fluids*, Vol. 52, No. 2, 2012, pp. 511–517. doi:10.1007/s00348-011-1241-9, URL https://doi.org/10.1007/s00348-011-1241-9.

[20] Rival, D. E., and Wong, J. G., "Measurements of vortex stretching on two-dimensional rotating plates with varying sweep," *10th International Symposium on Particle Image Velocimetry*, 2013.

[21] Wong, J. G., Kriegseis, J., and Rival, D. E., "An Investigation Into Vortex Growth and Stabilization for Two-Dimensional Plunging and Flapping Plates with Varying Sweep," *Journal of Fluids and Structures*, Vol. 43, 2013, pp. 231–243.

[22] Wong, J., and Rival, D., "Determining the relative stability of leading-edge vortices on nominally two-dimensional flapping profiles," *Journal of Fluid Mechanics*, Vol. 766, 2015, p. 611–625. doi:10.1017/jfm.2015.39.

[23] Jardin, T., and David, L., "Spanwise gradients in flow speed help stabilize leading-edge vortices on revolving wings," *Phys. Rev. E*, Vol. 90, 2014, p. 013011. doi:10.1103/PhysRevE.90.013011, URL https://link.aps.org/doi/10.1103/PhysRevE.90.013011.

[24] Klaassen van Oorschot, B., Mistick, E. A., and Tobalske, B. W., "Aerodynamic consequences of wing morphing during emulated take-off and gliding in birds," *Journal of Experimental Biology*, Vol. 219, No. 19, 2016, pp. 3146–3154. doi:10.1242/jeb.136721, URL http://jeb.biologists.org/content/219/19/3146.

[25] Hu, T., Wang, Z., and Gursul, I., "Passive control of roll oscillations of low-aspect-ratio wings using bleed," *Experiments in Fluids*, Vol. 55, No. 6, 2014, p. 1752. doi:10.1007/s00348-014-1752-2, URL https://doi.org/10.1007/s00348-014-1752-2.

[26] Greenblatt, D., "Fluidic Control of a Wing Tip Vortex," *AIAA Journal*, Vol. 50, No. 2, 2012, pp. 375–386. doi:10.2514/1.j051123, URL https://doi.org/10.2514/1.J051123.

[27] Boesch, G., Vo, H. D., Savard, B., Wanko-Tchatchouang, C., and Mureithi, N. W., "Flight Control Using Wing-Tip Plasma Actuation," *Journal of Aircraft*, Vol. 47, No. 6, 2010, pp. 1836–1846. doi:10.2514/1.44003, URL https://doi.org/10.2514/1.44003.

[28] Margaris, P., and Gursul, I., "Vortex topology of wing tip blowing," *Aerospace Science and Technology*, Vol. 14, No. 3, 2010, pp. 143 – 160. doi:https://doi.org/10.1016/j.ast.2009.11.008, URL http://www.sciencedirect.com/science/article/pii/S127096380900090X.

[29] Rizzetta, D. P., and Visbal, M. R., "Plasma Control for a Maneuvering Low-Aspect-Ratio Wing at Low Reynolds Number," *Journal of Fluids Engineering*, Vol. 134, No. 12, 2012, pp. 121104–121104–19. doi:10.1115/1.4007947, URL http://dx.doi.org/10.1115/1.4007947.

[30] Taira, K., and Colonius, T., "Effect of Tip Vortices in Low-Reynolds-Number Poststall Flow Control," *AIAA Journal*, Vol. 47, No. 3, 2009, pp. 749–756. doi:10.2514/1.40615, URL https://doi.org/10.2514/1.40615.

[31] Nikolic, V. R., "Optimal Movable Wing Tip Strake," *Journal of Aircraft*, Vol. 48, No. 1, 2011, pp. 335–341. doi:10.2514/1.c031014, URL https://doi.org/10.2514/1.C031014.

[32] Lee, T., and Pereira, J., "Modification of static-wing tip vortex via a slender half-delta wing," *Journal of Fluids and Structures*, Vol. 43, 2013, pp. 1 – 14. doi:https://doi.org/10.1016/j.jfluidstructs.2013.08.004, URL http://www.sciencedirect.com/science/article/pii/S0889974613001722.

[33] Slaouti, A., and Gerrard, J. H., "An experimental investigation of the end effects on the wake of a circular cylinder towed through water at low Reynolds numbers," *Journal of Fluid Mechanics*, Vol. 112, 1981, p. 297–314. doi:10.1017/S0022112081000414.

[34] Williamson, C. H. K., "Oblique and parallel modes of vortex shedding in the wake of a circular cylinder at low Reynolds numbers," *Journal of Fluid Mechanics*, Vol. 206, 1989, p. 579–627. doi:10.1017/S0022112089002429.

[35] Mueller, T. J., and DeLaurier, J. D., "Aerodynamics of Small Vehicles," *Annual Review of Fluid Mechanics*, Vol. 35, 2003, pp. 89–111.

[36] Granlund, K., Monnier, B., Ol, M., and Williams, D., "Airfoil Longitudinal Gust Response in Separated vs. Attached Flows," *Phys. Fluids*, Vol. 26, 2014, p. 027103.

[37] Greenblatt, D., Ḿueller-Vahl, H., Strangfeld, C., Medina, A., Ol, M. V., and Granlund, K. O., "High Advance-Ratio Airfoil Streamwise Oscillations: Wind Tunnel vs. Water Tunnel," *AIAA Paper 2016-1356*, 2016, pp. 1–19.

[38] Medina, A., Ol, M. V., Greenblatt, D., Ḿueller-Vahl, H., and Strangfeld, C., "High-Amplitude Surge of a Pitching Airfoil: Complementary Wind- and Water-Tunnel Measurements," *AIAA Journal*, Vol. 56, No. 4, 2018, pp. 1703–1709.

[39] Mulleners, K., Mancini, P., and Jones, A. R., "Flow Development on a Flat-Plate Wing Subjected to a Streamwise Acceleration," *AIAA Journal*, Vol. 55, No. 6, 2017, pp. 2118–2122.

[40] Lisoski, D. L. A., "Nominally 2-Dimensional Flow About a Normal Flat Plate," Ph.D. thesis, California Institute of Technology, 1993.

[41] Dickson, W. B., and Dickinson, M. H., "The effect of advance ratio on the aerodynamics of revolving wings," *Journal of Experimental Biology*, Vol. 207, No. 24, 2004, pp. 4269–4281. doi:10.1242/jeb.01266, URL `http://jeb.biologists.org/content/207/24/4269`.

[42] Harbig, R. R., Sheridan, J., and Thompson, M. C., "The role of advance ratio and aspect ratio in determining leading-edge vortex stability for flapping flight," *Journal of Fluid Mechanics*, Vol. 751, 2014, p. 71–105. doi:10.1017/jfm.2014.262.

[43] Jardin, T., "Coriolis Effect and the Attachment of the Leading Edge Vortex," *J. Fluid Mech.*, Vol. 820, 2017, pp. 312–340.

[44] Jardin, T., and Colonius, T., "On the Lift-Optimal Aspect Ratio of a Revolving Wing at Low Reynolds Number," *J. R. Soc. Interface*, Vol. 15, No. 143, 2018.

[45] Lee, Y. J., Lua, K. B., and Lim, T. T., "Aspect Ratio Effects on Revolving Wings with Rossby Number Consideration," *Bioinspir. Biomim.*, Vol. 11, No. 5, 2016, p. 056013.

[46] Bhat, S. S., Zhao, J., Sheridan, J., Hourigan, K., and Thompson, M. C., "Uncoupling the effects of aspect ratio, Reynolds number and Rossby number on a rotating insect-wing planform," *Journal of Fluid Mechanics*, Vol. 859, 2019, p. 921–948. doi:10.1017/jfm.2018.833.

[47] DeVoria, A. C., and Ringuette, M. J., "Vortex Formation And Saturation For Low-Aspect-Ratio Rotating Flat-Plate Fins," *Exp. Fluids*, Vol. 52, 2012, pp. 441–462.

[48] Merzkirch, W., *Flow Visualization*, 2nd ed., Academic Press, Inc., 1987.

[49] Jones, A. R., Pitt Ford, C. W., and Babinsky, H., "Three-Dimensional Effects on Sliding and Waving Wings," *J. Aircraft*, Vol. 48, No. 2, 2011, pp. 633–644.

[50] Yilmaz, T. O., and Rockwell, D., "Flow Structure on Finite-Span Wings Due to Pitch-Up Motion," *J. Fluid Mech.*, Vol. 691, 2012, pp. 518–545.

[51] Garmann, D. J., and Visbal, M. R., "A Numerical Study of Hovering Wings Undergoing Revolving or Translating Motions," *AIAA Paper 2013-3052*, 2013, pp. 1–21.

[52] Gursul, I., Gordnier, R., and Visbal, M., "Unsteady Aerodynamics of Nonslender Delta Wings," *Prog. Aerosp. Sci.*, Vol. 41, 2005, pp. 515–556.